

Supporting Information for Concentration–modulated global organizational chirality at the liquid/solid interface

Shu-Ying Li, ^{*a} Ting Chen, ^{b, c} Qi Chen ^a, Dong Wang ^{b, c}, and Guangshan Zhu^{*a}

^a Key Laboratory of Polyoxometalate and Reticular Material Chemistry of Ministry of Education,
Faculty of Chemistry, Northeast Normal University, Changchun 130024, P. R. China

^b Key Laboratory of Molecular Nanostructure and Nanotechnology and Beijing National
Laboratory for Molecular Sciences, Institute of Chemistry, Chinese Academy of Sciences (CAS),
Beijing 100190, P.R. China

^c University of Chinese Academy of Sciences, Beijing 100049, P. R. China.

Contents:

1. Molecular models for the enantioselective adsorption in CCW pattern.
2. Supplementary STM images for chiral amplification in the monolayer under control of majority-rules.
3. Supplementary STM images for concentration-modulated chiral amplification when the enantiomeric excess of *S*-OA in solution is fixed at 0.053.
4. Supplementary STM images for concentration-modulated chiral amplification when the enantiomeric excess of *S*-OA in solution is fixed at 0.102.

5. Correlation among molecular concentration, domain area and the number of trimers in one domain
6. Phase transition at higher concentration.
7. A collection of STM images obtained at low molecular concentration
8. Experimental methods

1. Molecular models for the enantioselective adsorption in CCW pattern.

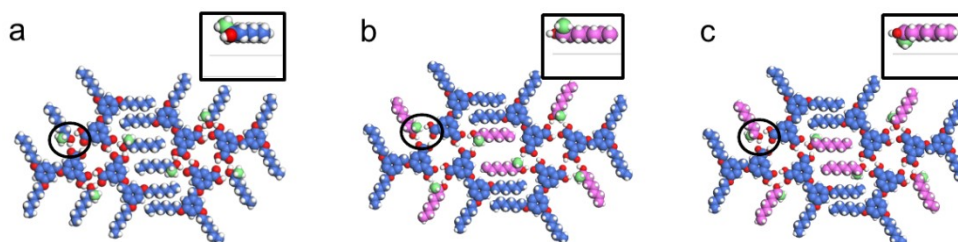


Figure S1. Molecular models for possible assembly modes on surface. (a) CCW pattern composed of *S*-OA with the methyl group upward relative to the substrate. (b) CCW assembly doped with *R*-OA at the expense of hydrogen bonding interactions between BIC molecules and alcohols. (c) CCW motif assembled by *R*-OA in which the methyl branch in alcohol points to the substrate. For clarity, *R*-OA in mismatched motif is modified in pink. Methyl group at the stereogenic center is painted green. The insets at the upper right depict the side view of the co-adsorbed 2-octanol in corresponding monolayer. Molecular mechanistic simulation reveals that the adsorption energies for assemblies in Figure S1a, 1b and 1c are $-25.6 \text{ kcal}\cdot\text{mol}^{-1}\cdot\text{nm}^2$, $-22.2 \text{ kcal}\cdot\text{mol}^{-1}\cdot\text{nm}^2$, $-24.5 \text{ kcal}\cdot\text{mol}^{-1}\cdot\text{nm}^2$, respectively. The first situation where CCW pattern constructed by *S*-OA with the methyl group upward relative to the substrate is energetically favored. As a result, *S*-OA triggers a preferential formation of CCW pattern. Similarly, *R*-OA prefers to assemble into CW pattern.

2. Supplementary STM images for chiral amplification in the monolayer under control of majority-rules.

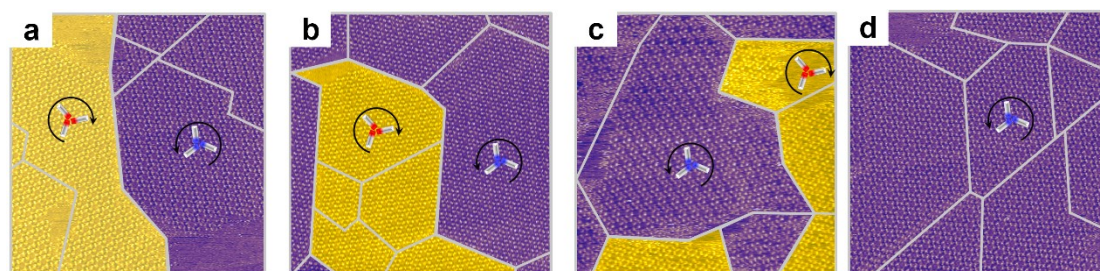


Figure S2. Supplementary STM images of BIC-C6 enantiomorphs assembled from premixed

solutions with different enantiomeric excess (*ee*) values. (a) *ee* = 0.012; (b) *ee* = 0.025; (c) *ee* = 0.053; (d) *ee* = 0.102. Concentration of BIC-C6 is 7.1×10^{-4} M. Image size is 100×100 nm². For clarity, CW domains are colored in yellow and CCW domains are painted purple. Gray lines separate adjacent domains. Average tunneling current (I_{set}) = 0.5–1 nA and bias voltage (V_{bias}) = 900 mV.

3. Supplementary STM images for concentration-modulated chiral amplification when the enantiomeric excess of *S*-OA in solution is fixed at 0.053.

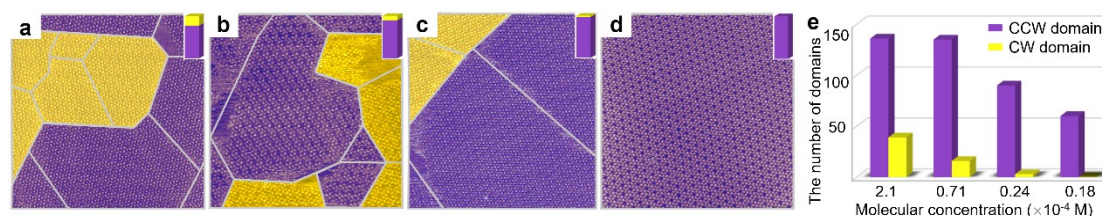


Figure S3. A selection of analyzed STM images displaying the controllable chiral amplification modulated by molecular concentration. Molecular concentrations: (a) 2.1×10^{-3} M; (b) 7.1×10^{-4} M; (c) 2.4×10^{-4} M; (d) 1.8×10^{-4} M. Enantiomeric excess of *S*-OA in solution is fixed at 0.053. CW domains are colored in yellow and CCW domains are painted purple. The bar graph in the upper right corner denotes the statistical relative proportion of the CW and CCW domain regions. Image size is 100×100 nm². Average tunneling current (I_{set}) = 0.5–1 nA and bias voltage (V_{bias}) = 900 mV. (e) Statistical graph representing the number of CW and CCW domain regions as a function of molecular concentration in solution.

4. Supplementary STM images for concentration-modulated chiral amplification when the enantiomeric excess of *S*-OA in solution is fixed at 0.102.

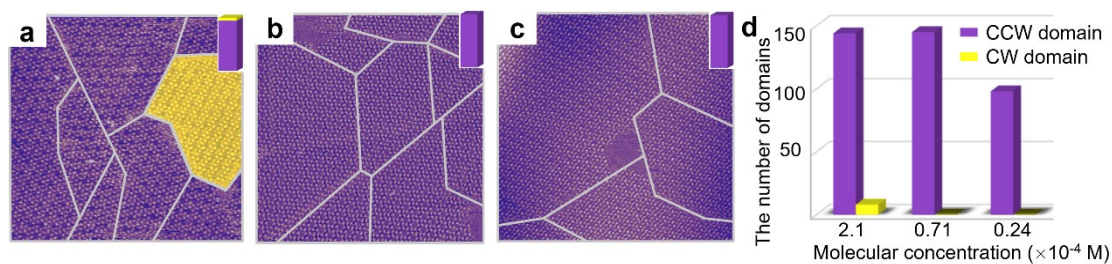


Figure S4. A selection of analyzed STM images displaying the controllable chiral amplification modulated by molecular concentration. Molecular concentrations: (a) 2.1×10^{-3} M; (b) 7.1×10^{-4} M; (c) 2.4×10^{-4} M. Enantiomeric excess of *S*-OA in solution is fixed at 0.102. CW domains are colored in yellow and CCW domains are painted purple. The bar graph in the upper right corner denotes the statistical relative proportion of the CW and CCW domain regions. Image size is 100×100 nm². Average tunneling current (I_{set}) = 0.5–1 nA and bias voltage (V_{bias}) = 900 mV. (d) Statistical graph representing the number of CW and CCW domain regions as a function of molecular concentration in solution.

5. Correlation among molecular concentration, domain area and the number of trimers in one domain

Molecular concentration (mol L ⁻¹)	2.1×10^{-3}	7.1×10^{-4}	2.4×10^{-4}	1.8×10^{-4}	1.0×10^{-4}
Average domain area (nm ²)	188	588	3454	4802	8070
Average numbers of structural units in one domain	20	63	372	516	868

Table S1. Statistical average domain size and number of trimers in one domain corresponding to a specified molecular concentration. The average number of trimers in one domain (n) is calculated from $n = A_{\text{domain}}/S_{\text{trimer}}$. A_{domain} is the average domain size. S_{trimer} is the unit area possessed by one

trimer on the substrate, which is measured to be 9.2 nm^2 .

6. Phase transition at higher concentration.

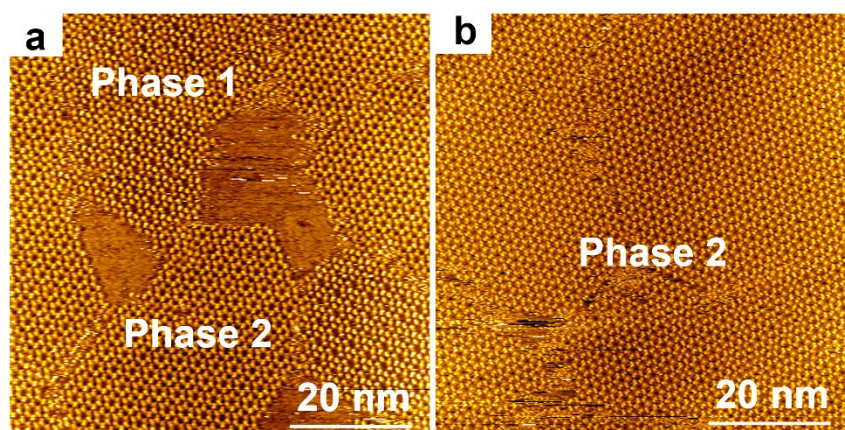


Figure S5. Phase transition occurs when the concentration of BIC-C6 is increased to 2.8×10^{-3} M.

7. A collection of STM images obtained at low molecular concentration.

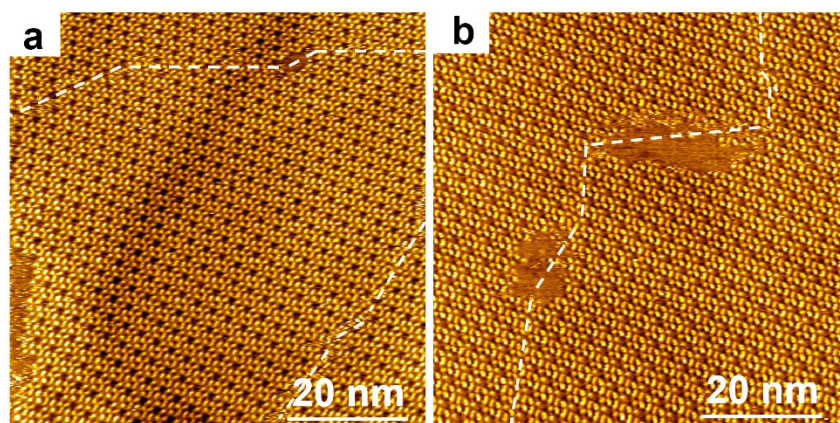


Figure S6. STM images of BIC-C6 assemblies at the liquid/solid interface with a low concentration of 1.8×10^{-4} M.

8. Experimental methods

Experimental details

BIC molecules were synthesized as described in previous literature^[1]. Chiral 2-octanol solvents were purchased from sigma-aldrich with purity of 99%. All the solvents were put to use directly. STM tips were prepared by mechanically cutting Pt/Ir wire (90/10). To obtain mixed enantiomer solvents, two enantiomers were first mixed together in a specific ratio in volume. Then BIC derivative was dissolved in the mixed solution with a concentration of 1×10^{-2} M. Solutions with different molecular concentration were obtained by diluting the original solution sequentially. To observe BIC networks, 1 μ L solution composed of BIC and solvent was applied to a freshly cleaved HOPG (grade ZYB) surface. All STM experiments were carried out using a PicoSPM (Agilent Technologies) system operating in constant-current mode at room temperature without further processing.

The experimental test generally lasts two hours for each sample. When solvent evaporation is considered, the mass of the 1 μ L solvent is reduced by 2.2×10^{-6} g after two hours. The concentration of solute increases from 1.0×10^{-4} M to 1.0027×10^{-4} M. Thus the concentration change caused by solvent evaporation is negligible and we suppose the solute concentration remains nearly constant during the experiment.

Statistical methods. At each concentration, distributions of enantiomorphs of BIC-C6 on surfaces were recorded based on at least three samples. For each sample, typically more than 20 large-scale STM images (100×100 nm²) were obtained at different locations.

Molecular modeling. Molecular mechanistic simulations were carried out with the molecular package TINKER using the MMFF force field^[2]. 2D packing models of BIC derivative were built according to the STM images. During optimization the BIC monolayers are placed 0.35 nm above

the upper layer of a two-layer sheet of graphite keeping the alkyl chains in BIC parallel to the directions of graphite symmetry axes, and the graphite was frozen. As processed in previous literature^[3], the calculated energy from MM simulations is divided by the area possessed by the hexagonal network.

References

- [1] J. R. Gong, S. B. Lei, L. J. Wan, G. J. Deng, Q. H. Fan, C. L. Bai, *Chem. Mater.* **2003**, *15*, 3098-3104.
- [2] a) C. E. Kundrot, J. W. Ponder, F. M. Richards, *J. Comput. Chem.* **1991**, *12*, 402-409; b) T. A. Halgren, *J. Comput. Chem.* **1996**, *17*, 490-519; c) P. Ren, C. Wu, J. W. Ponder, *J. Chem. Theory Comput.* **2011**, *7*, 3143-3161.
- [3] C.-A. Palma, M. Bonini, A. Llanes-Pallas, T. Breiner, M. Prato, D. Bonifazi, P. Samorì, *Chem. Commun.* **2008**, 5289-5291.